Indian Journal of Radio & Space Physics
Vol 41, April 2012, pp 168-183

Equatorial spread F development and quiet time variability under solar minimum conditions

M A Abdu

National Institute for Space Research - INPE, Sao Jose dos Campos, SP, Brazil

E-mail: maabdu@dae.inpe.br

Received October 2011; accepted 29 March 2012

This paper provides a brief review of our current understanding of the equatorial spread F irregularity (ESF) development related to the diverse processes that control or influence the spatial-temporal distribution and day-to-day variability in the occurrence of the irregularities during solar minimum conditions. The sunset electrodynamics processes leading to the ESF development are briefly explained highlighting the main ESF driving forces and their relative importance during solar maximum and minimum conditions. Whereas, its post sunset occurrence characterizes the quiet time solar maximum conditions, the ESF occurrence dominates the midnight-post midnight/pre sunrise hours under solar minimum conditions. The role of the evening pre-reversal enhancement in vertical drift (PRE) relative to that of a gravity wave precursor seed, for instability growth in the ESF development, is discussed. Their relative roles vary with the level of solar activity, such that the ESF occurrence pattern tends to have larger dependence on gravity wave distribution during solar minimum conditions (than during solar maximum), which points to the importance of pursuing studies using the immense data base accumulated during the prolonged solar minimum phase that just passed. While the solar minimum spread F irregularities driven by the equatorial electrodynamics processes might be connected to the gravity waves originating from tropical convective sources, the post midnight spread F of the low-latitude region appears to be ruled mainly by the medium-scale travelling ionospheric disturbance (MSTID) of mid-latitude origin

Keywords: Equatorial spread F (ESF) irregularity, Low-latitude spread F, Solar minimum condition, Gravity wave seed, Pre-reversal enhancement in vertical drift (PRE), Medium-scale travelling ionospheric disturbance (MSTID)

PACS Nos: *94.20.dj; 94.20.dt; 96.60.qd*

1 Introduction

The equatorial nighttime F-region plasma irregularities has been the subject of extensive investigation during the last several decades since its discovery by Booker & Wells[1] as range spreading F-layer trace in ionograms over the equatorial station Huancayo. Its generic name, the equatorial spread F (ESF) signifies the occurrence of a composite of magnetic field aligned plasma irregularities (or plasma structures) with cross field line scale sizes ranging from a few meters to a few hundreds of kilometers, so that the diagnostics of the entire irregularity spectrum is possible only by means of wide ranging techniques. Ground based as well as space borne instruments, in radio and optical bands, remote sounding and *in situ* modes, have been extensively utilized in recent years to investigate the different characteristics of ESF. The interference and interruptions to space based application systems of various kinds (such as the use of GPS satellites in various applications) posed by these irregularity structures highlight the need to predict their occurrences in space and time, which demands detailed understanding of the mechanisms of their generation and decay processes as well their variability at different time scales. As a result of the observational and modeling/simulation studies conducted so far, there is a rather clear picture of their spatial and temporal distributions over the globe in wide ranging scales, their effects on space and ground based radio communication systems, and an in-depth understanding of the process and mechanisms that control their development (Refs 2-27 and references therein). However, there is no sufficient understanding of the nature of the large degree of the short term/day-to-day variability in the dynamical conditions of the background ionosphere-thermosphere system that control the ESF irregularity development and its variabilities at different time scales. Such variabilities can be broadly classified as: (1) long term variation dependent on solar activity cycle, (2) medium term variation at monthly and

seasonal scales, and (3) shorter term variability on the scale of a day or less. The long term variation is understood to be basically driven by a corresponding variation in the evening pre-reversal zonal electric field/vertical drift enhancement (PRE) that is controlled by the solar EUV flux, represented by the proxy index F10.7 (Refs 18,28,29). The medium term variations arise from a longitude dependent seasonal effect, which is controlled to a first degree by the magnetic declination angle that varies with longitude[6,13,30], as well as by the solar declination angle that varies with season. Abdu *et al.*[6] showed that the degree of simultaneity of the sunset at the conjugate E-layers (connected to the equatorial F-layer bottom side), that is, the degree of alignment of the sunset terminator with the magnetic meridian, controls the intensity of the PRE to the first order so that the near alignment condition produces larger PRE intensity and hence more intense ESF[6,31,32]. Since the amplitude of the PRE largely controls the ESF intensity, a longitude dependent seasonal variation that is present in the PRE is also present in ESF. Modulation on the seasonal/longitude variation due to upward propagating GWs, originating from tropospheric convective sources, as inferred from the movement of the ITCZ (inter-tropical convergence zone), has been proposed by different researchers[14,22,33], based largely on statistical analyses of the data. Based on case studies, the role of such gravity waves is now increasingly believed to be an important source of ESF day-to-day variability as well[34-36]. The question on the precise nature of the control of gravity waves on the ESF variability now remains to be one of the least tackled and therefore, a most challenging scientific problem to be addressed in this field.

The sources and degrees of the short-term variability, apart from being longitude dependent, are also dependent upon the epoch of the year, and the level of solar activity. The latter aspect, namely, the solar activity dependent causes ESF variability is of specific relevance for this paper. The dominant sources of ESF variability during a period of extremely low solar activity have been discussed as compared to those that characterize the solar maximum conditions. The factors, will also be discussed, which are believed to be controlling the post midnight F region irregularity development and variability that tend to dominate the solar minimum period as different from the factors that control the post-sunset ESF processes that seem to dominate the solar maximum period. Before the various causes of ESF variability are discussed, it is opportune to present a brief general description of the processes operating in the ESF development under quiet conditions (Kp < 2+)

2 General considerations on ESF development and variability

A schematic of the electrodynamics coupling processes responsible for the ESF post-sunset development is shown in Fig. 1. The ESF occurs following a rapid rise of the F-layer (by vertical plasma drift) under the action of the evening pre-reversal enhancement in zonal (eastward) electric field (PRE). The F-layer dynamo intensification at sunset is responsible for the PRE development, which begins with the start of sunset at conjugate E-layers that are coupled to the equatorial F-layer[6]. The E-layer conductivity local time/longitude gradient (indicated as SS.$\Delta\Sigma$ in the figure) and the thermospheric zonal wind (also indicated in the figure) which is eastward in the evening play their crucial roles in electrodynamic coupling processes leading to the PRE development[37-39]. The steep bottom-side density gradient of the F-layer, rising under the PRE, becomes unstable to density perturbations leading to instability growth by the Rayleigh-Taylor (R-T) mechanism by which the rarified plasma of the F-layer bottom side rises up to the topside ionosphere in the form of flux tube aligned plasma depletions/plasma bubbles having scale sizes of tens to hundreds of kilometers. With the nonlinear growth of these bubble, secondary instabilities take over in cascading process leading to the irregularity structures, also magnetic field aligned, down to meter sizes[4], the entire process constituting

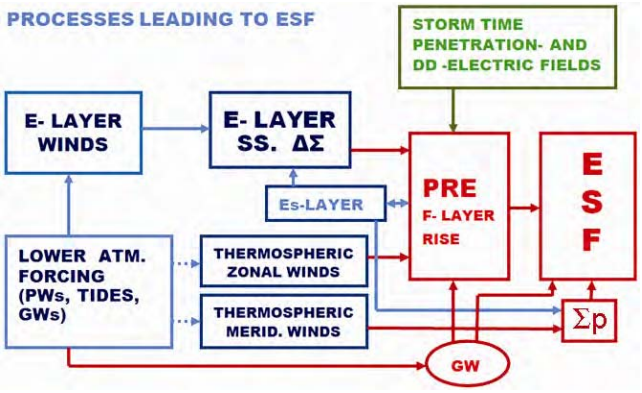

Fig. 1 — A scheme of the coupling processes leading to equatorial spread F/plasma bubble irregularity development

the development of an ESF event. VHF radar diagnostics have shown that the irregularities develop close to or before the terminator passage at the field line apex in the F-region and the structures move eastward[26,40].

The ESF instability growth, believed to be driven by the R-T process through collisional interchange instability (CII) mechanism leads to bubble irregularity development through generation of polarization electric field whose growth rate is governed by the Eq. (Ref. 35):

$$\partial\delta E_x/\partial t - \gamma_R \delta E_x = S_x \quad \ldots (1)$$

$$\gamma_R = (-E_{0x}/B_0 - W_y + g/\nu_i)/l_0 \quad \ldots (2)$$

$$S_x \approx B_0 \Delta U_{0x}/l_0 \, (\delta W_y/\kappa_i - \delta W_x) \quad \ldots (3)$$

$$1/l_0 = d\log n_0/dy \quad \ldots (4)$$

where, γ_R is the linear growth rate for the polarization electric field; E_{ox}, the prereversal zonal electric field (positive westward); ΔU_{0x}, differential ion-neutral zonal velocity; W_y, the vertical neutral wind; $\delta W_{x,y}$, the gravity wave associated winds; n_o, the electron density; and κ_i, the ratio of the ion gyrofrequency, Ω_i, to ion-neutral collision frequency, ν_{in} (Refs 34,35). The nonlinear growth of the instability to form vertically extended topside bubbles is controlled also by the integrated conductivity of the unstable flux tube[17,41,42] which is controlled by meridional winds, as indicated in Fig. 1, but not considered in the Eq. (1). A trans-equatorial wind causes an uplift of F-region plasma of the upwind hemisphere and therefore, a reduction in the integrated conductivity that happens to be smaller than the increase of the integrated conductivity on the downwind hemisphere. This is due to the unequal molecular ion distribution in the conjugate F-region caused by the wind as explained by Maruyama[41]. Thus, there is a net increase in the field line integrated conductivity. The instability growth rate by including field line integrated conductivity has been represented in terms of flux tube integrated parameters by Maruyama[41] and Sultan[17].

Also, indicated in the schematic of Fig. 1, is the lower atmosphere forcing involving upward propagating waves in the form of tidal modes, gravity waves and planetary waves. The upward propagating tidal modes, often modulated by planetary waves, regulate the E-layer winds that generate the dynamo electric field, as well as the E-layer conductivity longitudinal gradient at sunset that controls the PRE development, and hence, the ESF growth[43]. The gravity waves originating from sources of tropospheric convection, in their upward propagation to thermospheric heights, are increasingly believed to be the seed perturbations required for ESF development[14,34-36].

Based on the above discussion, the most important parameters that control the development of an ESF event are the following:

1. The F-region plasma vertical drift/zonal electric field in the evening hours, that is, the evening pre-reversal enhancement in the vertical drift arising from the F-layer dynamo;
2. Initial perturbations in electron density and polarization electric fields at the F-layer bottom-side gradient region as precursor seed for the instability growth;
3. Thermospheric meridional/trans-equatorial winds that control the field line integrated conductivity of the potentially unstable flux tubes;
4. Density gradient of the F-layer bottom-side.

Notwithstanding the fact that these parameters are in some way (or indirectly) interdependent, the variability in any of them could cause a corresponding variability in the ESF. The variabilities that can arise from the parameters 3 and 4 are not discussed in this paper as they are observationally less studied than the others.

The evening PRE vertical drift (of parameter 1) represented by the term $-E_{0x}/B_0$ in the linear growth rate expression γ_R contained in Eq. (1), has been by far the most directly identified control parameter considered in the investigations on the ESF variability[7,18,44,45]. The importance of a seed perturbation in the form of gravity waves has also been the subject of investigation. Based on the available results, it appears that a competing and complementary role of the PRE and GWs in the ESF development can be identified in case studies as well as in statistical data. Some results on this important question are presented below. It may be noted that the PRE presents significant dependence on solar flux[29,46,47], its value being around four times higher during high solar flux years (solar maximum) as compared to its value during low solar flux (solar minimum) years. Little is known about the solar flux dependence of gravity waves (GWs). However, its role in the ESF processes appears to be more easily observable / detectable during the low solar flux years when the PRE is expressively weaker than it is during

the solar maximum years when the PRE dominates the ESF process. As a result, it turns out that the recent long duration solar minimum epoch provides an ideal opportunity to investigate the roles of GWS in the ESF short term/day-to-day variability. An important consequence of the enhanced role of GWS in the ESF processes during years of low solar flux is that post midnight spread F occurrence is, in general, and especially during solstice months, more frequent than the post-sunset events.

3 Evening pre-reversal vertical drift and ESF

The evening zonal electric field pre-reversal enhancement (PRE), that is, the enhanced vertical drift, contributes to the linear growth rate γ_R in two ways: (a) through the vertical drift term, and (b) through the layer height, a raised (lowered) layer with reduced (increased) collision frequency causing enhanced (reduced) contribution from the g/ν_i term [Eq. (1)]. A larger γ_R is helpful for a more intense nonlinear growth of the polarization electric field and hence, to larger vertical growth of the ESF/bubble structure, which is a measure of the intensity of an event. The degree to which the PRE controls the spread F (SF) intensity is illustrated in Fig. 2 (adopted from Chapagain *et al.*[45]). In this figure, the PRE vertical drift is shown as a function of the solar flux index (F10.7) for different degree of SF intensity over Jicamarca. For the case of weak spread F (generally confined to the bottom-side) as also for the plume type spread F (that extends to the topside), the vertical drift at the SF onset time, as also the PRE amplitude, increases with solar flux. Here, the SF intensity is measured in terms of the height extension of the radar echoes, and it is seen that for any given solar flux value the vertical drift at the SF onset time as well as the PRE amplitude is higher for plume type SF than for weak SF. They also present some degree of seasonal dependence. There is, however, a large degree of scatter in the relationship, which may point to the importance of other influencing factors (e.g. the amplitude of the seed perturbation required for the instability growth) in the control of the ESF intensity and its variability.

A more direct way of verifying the control of the ESF by vertical drift is presented in Fig. 3 (adopted from Su *et al.*[44]) that shows the monthly variation of

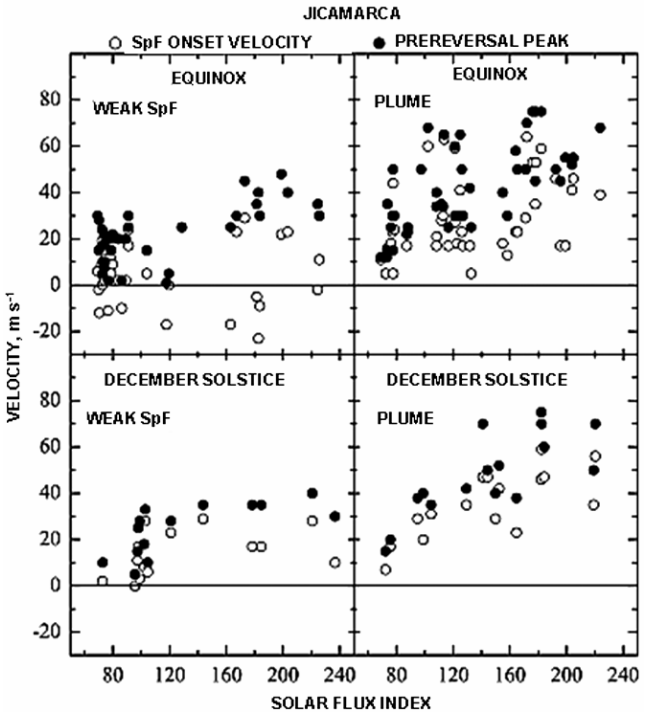

Fig. 2 — Scatter plots of weak spread F and plume onset velocities and corresponding pre-reversal drift peaks as a function of solar flux index (Chapagain et al.[45])

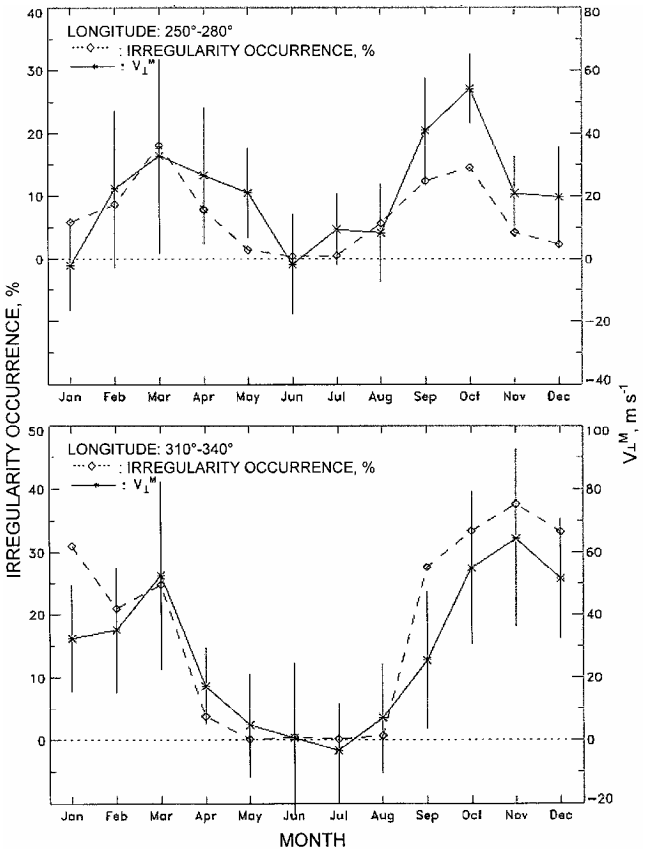

Fig. 3 — Comparison of the post-sunset vertical drift velocities and the irregularity occurrences as monthly mean values, as observed by ROCSAT -1 at two longitudes 250–280° and 310–340° (Su *et al.*[44])

global equatorial irregularity occurrence and the corresponding post-sunset vertical plasma drift as obtained from the ROCSAT-1 observation at 600 km (in the topside) for two longitude sectors, 250°-380° and 310°-340. Excellent correspondence can be noted at both longitude sectors between the irregularity occurrence and vertical drift. From the smooth pattern of the seasonal variation of the two parameters, that is, longitude dependent as a function of magnetic declination, Su *et al.*[44] argued that the ESF occurrence pattern as revealed by the ROCSAT-1 can be fully explained on the basis of the vertical drift without the need to invoke any influence from a seed perturbation due to gravity waves. The result in Fig. 3 shows that large vertical drifts are necessary for significant degree of irregularity occurrence in both longitude sectors. For example, vertical drifts of the order of 60 m s^{-1} are associated with monthly irregularity occurrence of 35% in the Atlantic longitude sector and 15% in the Pacific sector during the Oct-Nov period of the high to medium solar activity conditions of the measurement. These irregularities arise from the equatorial plasma depletion structure vertical growth attaining at least 600 km of altitude for which significant vertical drifts are required as is indeed observed. The duration of the evening vertical drift and its time integrated effect on the resulting F-layer heights could also control the degree of irregularity occurrence. Any possible gravity waves role in the irregularity growth is likely to be more difficult to be observed for increasing intensity of the pre-reversal vertical drift.

The control of the plasma bubble vertical growth by the PRE can be illustrated from the results shown in Fig. 4**,** adopted from Abdu *et al.*[8]. This figure shows the F-region vertical drifts at the three sites of the conjugate point equatorial experiment (COPEX) campaign conducted in Brazil during October-December 2002. The drifts are obtained from the digisondes operated at these sites and their mean values for different groups of days are plotted in the figure (details on the drift calculation available in Abdu *et al.*[8]). The pre-reversal enhancement in the vertical drift can be noted starting near 2100 hrs UT (~1730 hrs LT). Through field line mapping, the plasma bubble rise velocity over the dip equator determines the onset time of the ESF at latitudes farther away from the dip equator, an earlier spread F onset resulting from a higher bubble rise velocity. Four groups of days sorted out on considerations of systematic increase in SF onset time at locations (latitudes) farther away from the dip equator are shown in the successive four panels. The locations considered are: Campo Grande (20.5°S, 54.7°W, dip angle -22.3°) and Cachoeira Paulista (22.7°S; 45°W. dip angle -33.7°). The average ΣKp values corresponding to the sorted group of days are also shown in these panels. Based on the flux tube aligned bubble development, the spread F occurrence at early post-sunset local times (before 2000 hrs LT) over Cachoeira Paulista (CP) corresponds to a rather fast vertical bubble rise velocity (>150 m s^{-1}) over the equator. For this case, the mean Vz peak values (Vzp)

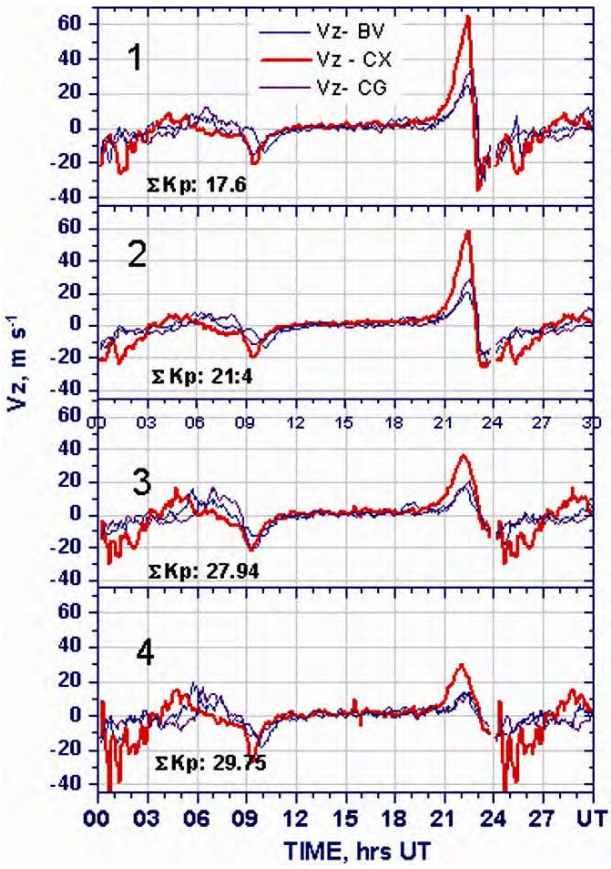

Fig. 4 — Mean vertical drift velocities over the three COPEX sites plotted for different groups of days for: (Panel 1) the cases of early spread F occurrence (at or before 2000 hrs LT) over Cachoeira Paulista; (Panel 2) the group of days when SF occurred at and before 2200 hrs LT over CP; (Panel 3) the group of days when SF did not occur before midnight over Cachoeira Paulista; and (Panel 4) the group of days when SF did not occur over Campo Grande and CP. (ΣKp: the daily sum of the 3-hourly Kp values representing the mean value for the days considered) (Station names are BV: Boa Vista; CX: Cachimbo; and CG: Campo Grande. In the x-axis, the LT exceeding 24 hours corresponds to a new day so that 24 should be subtracted from those values) (Abdu *et al.*[8])

over Cachimbo (near the dip equator) in the top panel is ~ 62 m s^{-1}. For a second group of days corresponding to spread F events occurring at and before 2200 hrs LT over CP, the mean Vzp is only slightly smaller, being 59 m s^{-1}, in panel 2. The results in panel 3 is for the case of spread F not occurring till midnight over CP (which signifies that the vertical bubble growth over the dip equator did not attain till midnight an apex altitude of 900 km that is field line mapped to the bottom-side F-region over CP), which corresponds to bubble rise velocity not exceeding 40 m s^{-1}. For this case, the Vzp over Cachimbo is around 35 m s^{-1}. The field line apex height for Campo Grande bottom-side F-region is ~ 650 km. For the cases of post-sunset spread F not occurring over Campo Grande, the mean Vzp in panel 4 is 30 m s^{-1}, which suggests that bubble vertical growth to ~650 km could be possible when the pre-reversal vertical drift is higher than this value. For the cases of non occurrence of spread F over the equator (and therefore, at the off equatorial sites as well), the mean Vzp (not shown here) was just 22 m s^{-1}, which can be considered to be the threshold minimum below which bottom-side spread F did not occur over the equator for this observational interval. Thus, it is noted that in statistical terms, the average Vzp presents a trend suggesting its systematic control on the spread F /bubble vertical growth, with the lowest Vzp (22 m s^{-1}) for the case of spread F totally absent (zero vertical growth) to the highest Vzp (~ 60 m s^{-1}) for a rapid vertical growth of the bubble (with rise velocity >150 m s^{-1}) over the equator. It is relevant to mention here that threshold condition on the evening pre-reversal vertical drift for UHF and L-band scintillation occurrence in the Peruvian sector have been discussed by Anderson *et al.*[48]. In Fig. 4, the Vz variations are also shown over the conjugate sites of Cachimbo (Campo Grande and Boa Vista) where the Vzp values are significantly smaller than over equator with a small asymmetry suggesting the presence of a generally weak trans-equatorial wind in the F-layer bottom-side, which might indicate that the control of the bubble rise velocity by the PRE intensity demonstrated above is largely unaffected by trans-equatorial winds.

4 Gravity wave seeding of the ESF

Atmospheric gravity waves (GWs) propagating at thermospheric and F-region heights can originate from different sources. Of special interest for the ESF studies are those originating from tropospheric convective sources that dissipate energy and momentum at E- and F-region heights[35,49,50]. Depending upon the propagation vector, the gravity waves in the thermosphere can modulate the F-region structure and dynamics in different ways, some of which having direct impact on the ESF development. The consequent effects can be classified as:

1 Large scale GWs can modulate the post dusk sector F-layer heights through large undulations in electron density iso-lines, whereby the elevated bottom-side density gradient regions become unstable to GRTI (generalized Rayleigh-Taylor instability) with large instability growth rates[51];

2 It is well known that the background thermospheric zonal wind, that turns eastward in the evening, is the major driver of the PRE. A superposition of this background zonal wind with a perturbation zonal wind due to GWs can cause large increase or decrease of the PRE amplitude depending upon the GW phase that in turn can lead to enhanced or reduced instability growth rate through $(E_{0x}/B_0)/l_0$. The modified PRE associated raise or descent of the F-layer could also enhance or reduce the gravitational RTI growth rate factor $(g/\nu_i l_0)$. A GW imposed zonal perturbation wind in the post-sunset hours could modify also the wind driven instability growth rate such as that discussed by Kudeki *et al.*[52];

3 GWs can seed the instability by providing perturbations in the bottom side electron density in which polarization electric field grows in such a way that a further growth of a density depletion, caused by the polarization electric field, contributes to intensify the causative polarization electric field through a cycle of positive feedback, constituting the instability growth process. This process, in particular, would require that the GW propagation vector be aligned along the dip equator, that is, the phase front of the wave be aligned with magnetic meridian for most favourable condition for instability growth (as pointed out by Tsunoda[14]).

Here, the focus is on the role of GWs in the direct seeding of the instability. In order to examine any possible role of GWs in the initiation of post-sunset spread F/bubble irregularities, it is first necessary to look for precursor signatures in the form of perturbation in the F-layer density or iso-density

heights during the evening hours that just precede the spread F onset. It is known that the PRE is the most basic requirement for the spread F to develop in such a way that its intensity needs to attain a minimum threshold limit for the instability to grow. For a given background, ionosphere-thermosphere conditions that threshold limit could dependent on the intensity of the GW seed perturbation (along possibly with other factors indicated in Fig. 1). A case study is presented below showing the complementary roles of the GW precursor and the PRE in the instability growth leading to spread F development. The study is based on an analysis of radar and digisonde data from a recent SpreadFEx Campaign conducted in Brazil[36]. Figure 5(a) (adopted from Abdu *et al.*[34]) shows for 23-24 October 2005 over Sao Luis, the RTI map of 5-m plasma structures from a 30 MHz radar (in the top panel). The successive lower panels show the F-layer true heights at plasma frequencies 5, 6, 7 and 8 MHz (from digisonde), the vertical drift, the height oscillations for periods less than ~3 hours (over Fortaleza), and finally the collisional interchange instability (CII) growth rate factor (V_z/l_0 calculated from the upper two panels). It may be noted that the irregularity plumes (indicating topside bubble structure) developed within ~ 30 minutes after the peak in the Vz, which is consistent with the peak growth rate factor of $5x10^{-3}$ s^{-1} for this case. It may, further, be noted that the precursor perturbations in the dhF parameter at 5-8 MHz do not clearly indicate the presence of significant gravity waves (although some estimation of the GW parameters can be obtained from them). This contrasts with the results of 24 October that clearly indicate the presence of significant GWs as can be verified from the downward phase propagation in the height oscillations (dhF) around the sunset hours [panel 2 from bottom in Fig. 5(b)]. On this evening, topside bubbles did not develop promptly which can be attributed to the weaker PRE and lower F-layer heights on this evening[34]. The radar plume that developed after 2220 hrs UT (1920 hrs LT) was mostly confined to bottom-side. To explain these results, a simulation of the CII growth by the Rayleigh-Taylor (R-T) mechanism was performed that took into account the polarization electric field development from gravity wave winds together with the background ionospheric conditions, such as the pre-reversal zonal electric field, the F-layer heights and bottom-side density gradient[34,35]. The simulation that used the background ionospheric conditions of 23 October together with the estimated GW winds produced an instability polarization electric linear growth that attained exponential rate (not shown here) within a short time (<30 min from the instability initiation), which is consistent with the topside plume structure that promptly developed on this evening. When the same simulation was done for the background conditions of 24 October, but using the GW winds as on 23 October, the polarization electric field did not begin to grow till after one hour. However, when the GW winds of 24 October, (which was around 3 times larger than that of the 23 October), was used in the calculation the growth rate attained significant values (but still at a slower rate than on 23 October), which is consistent with the limited plume growth that was observed. Thus, this result clearly demonstrates the role of GW winds in seeding the spread F instability process. It should be pointed out that the amplitude of the PRE in this latter case [Fig. 5(b)] was relatively smaller (< 20 m s^{-1}) than the usual statistical threshold limit for fully developed plasma bubbles which has been found to be ~ 35 m $s^{-1}$for solar maximum equinoctial months[53]. A few other cases analyzed also conformed to these results. The above results, though based on limited case studies, would seem to suggest that for the cases of ESF development that follow comparatively large PRE, the role of an instability seed by GWs is close to or below a threshold limit normally detectable by a digisonde. On the other hand, when the PRE is relatively weak, the role of GWs seeding is easier to be detected as precursor oscillations in the F-layer height by digisondes.

5 Post-midnight spread F irregularities

There has been increasing interest, in recent years, in the investigation on the occurrence of post-midnight / pre-sunrise spread F irregularities, aiming at improving our understanding of their dynamical characteristics and generation mechanism[54-57]. While a part of these irregularities arise from delayed functioning of the well-known post-sunset irregularity development mechanism and the longer persistence of the irregularities, a major part seems to arise from other processes that operate during the post-midnight hours. One component of its occurrence is controlled by magnetic activity, as the efficiency for disturbance electric field penetration to equatorial latitudes is large at these hours[18]. Their occurrence rate, in general, increases with decrease of solar flux[58,59]. The seasonal/longitude and solar activity dependent

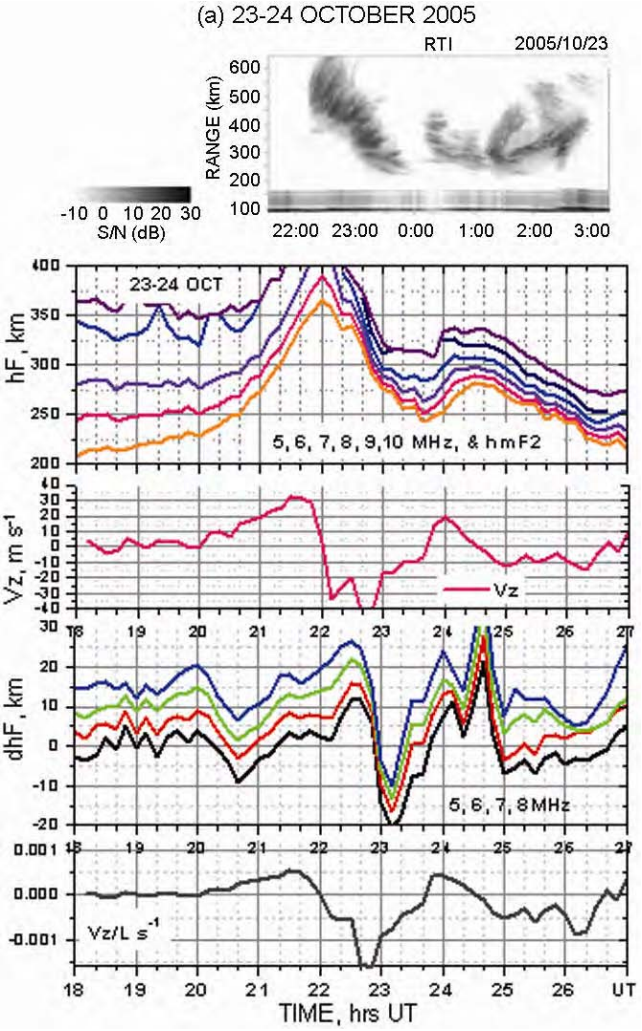

Fig. 5(a) — Plots for the 23–24 October 2005: (top panel) RTI map of 5-m irregularity distribution as observed by the 30 MHz radar over Sao Luis; (panel 2 from top) F-layer true heights at plasma frequencies 5, 6, 7 and 8 MHz over Fortaleza; (panel 3 from top) Mean of the drift velocities calculated as d(hF)/dt at frequencies 5, 6, 7, and 8 MHz; (panel 4 from top) Band-pass filtered (for 20 min to 3 -h periods) height oscillations at frequencies 5, 6, 7, and 8 MHz; (bottom panel) Instability growth rate due to the term V z/L of the instability linear growth rate factor (Abdu *et al.*[34])

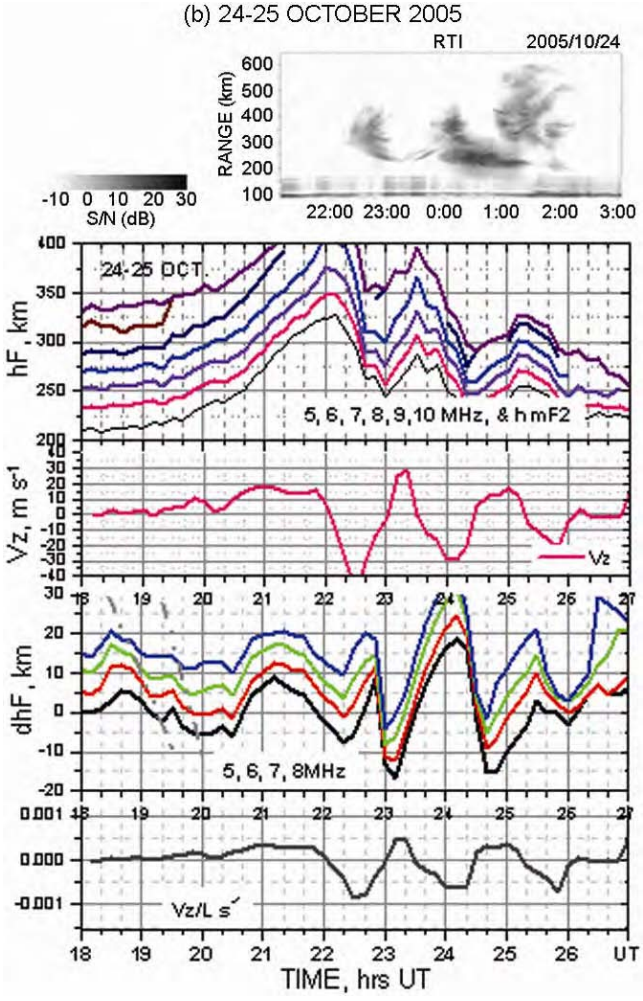

Fig. 5(b) — Plots for the 24–25 October 2005: (top panel) RTI map of 5-m irregularity distribution as observed by the 30 MHz radar over Sao Luis; (panel 2 from top) F-layer true heights at plasma frequencies 5, 6, 7 and 8 MHz over Fortaleza; (panel 3 from top) Mean of the drift velocities calculated as d(hF)/dt at frequencies 5, 6, 7, and 8 MHz; (panel 4 from top) Band-pass filtered (for 20 min to 3 -h periods) height oscillations at frequencies 5, 6, 7, and 8 MHz; (bottom panel) Instability growth rate due to the term V z/L of the instability linear growth rate factor (Abdu *et al.*[34])

characteristics of these irregularities, in general, appear to vary from equator to low-latitudes.

Pre-sunrise spread F over a near equatorial site Fortaleza, Brazil, during 1994-1995, a near-solar minimum epoch, was investigated by MacDougall *et al.*[60]. Its occurrence presented two seasonal peaks, one of them being centered in the December solstice (with 90% occurrence) and the other around the June solstice (with > 70% occurrence). The irregularities drifted eastward and were found to be collocated with F-layer bottom-side bulges as diagnosed by a CADI (Canadian Digital Advanced Ionosonde). Measurement of the irregularity zonal drift indicated that the bottom-side bulges are unstable to gradient drift instability with relatively slow growth rate. Over Cachoeira Paulista, which is close to the southern EIA crest in the same longitude sector, the post-midnight spread F in the June solstice months (May Jun, Jul, Aug) of low solar flux years reached similar occurrence rate (60-70%) as that of Fortaleza (Fig. 6). Shown in Fig. 6 (adopted from Candido *et al.*[59]) is the

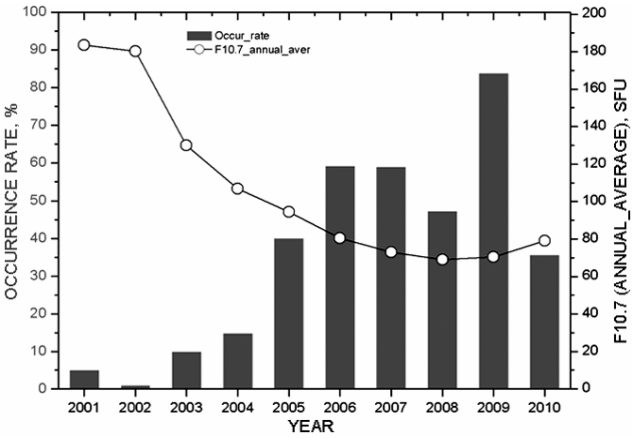

Fig. 6 — Spread F occurrence rate during quiet nights (May–August average) at Cachoeira Paulista between 2001 and 2010 and F10.7 index [full bars are the Spread F occurrence percentage under quiet conditions (∑Kp < 24) with respect to the total number of nights of ionospheric data, and the unfilled bars (measured from zero) represent the percentage of Spread F nights under quiet conditions (∑Kp < 24) with respect to the total number of quiet nights, using data from 1 May to 31 August (Candido *et al.*[59])]

occurrence rate of post-midnight spread F in the June solstice months over CP as a function of the solar flux index F10.7. It is noted that the occurrence rate of <5% during solar maximum (with F10.7 ~180 units) increases up to 80% for solar minimum with F10.7 values of around 70 flux unit. The available statistics for Fortaleza[31] also show a similar negative dependence of the post-midnight spread F on F107. In the case of December solstice, the available results from published works[31,60] show that the post-midnight spread F occurrence rate increases from high solar flux to low solar flux years, being ~50% and 90%, respectively near 0300 hrs LT. No such statistics are now available for the December solstice months over CP. So, these results show that in the Brazilian sector, the post-midnight irregularities occur, in general, more frequently during solar minimum years than during solar maximum years.

The statistics of the post-midnight spread F for June months over Jicamarca is shown in Fig. 7

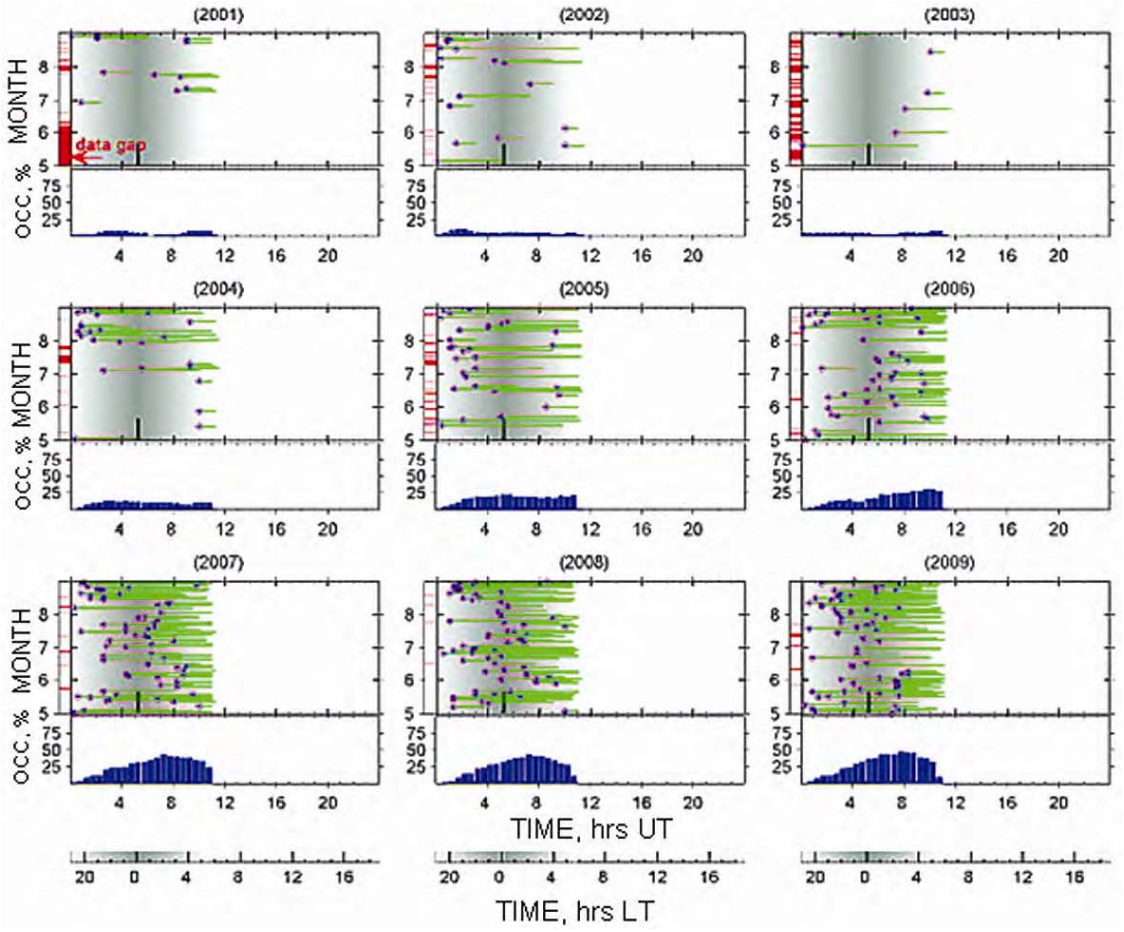

Fig. 7 — Onset time (blue dots) and the duration (green horizontal lines stretching from the dots) distribution of spread F over Jicamarca during 2001–2009 [Occurrence probability *vs* UT is shown at the bottom part of each plot. (Li *et al.*[58])

(adopted from Li *et al.*[58]). Here, it may be noted that the occurrence rate peaks near 0300 hrs LT (0800 hrs UT) and it increases from near 0% in solar maximum (2001) to about 50% in solar minimum (2009). This confirms that the solar activity trend in the occurrence rate of the post-midnight irregularities in June solstice months is similar in the entire South American sector.

The structure and dynamics of the post-midnight irregularities were investigated, using the equatorial atmospheric radar (EAR) in Indonesia and the Communication/Navigation Outage Forecasting System (C/NOFS) satellite, by Yokoyama *et al.*[56,57]. Their observations were also conducted during June solstice months of solar minimum at 10.36°S dip latitude in the Asian sector[61]. They identified two types of irregularities both propagating usually westward. One type presented sharp upwelling plumes near local midnight which might be produced by the R-T instability mechanism under conditions made favourable, according to the authors, by the converging winds of the midnight temperature maximum (MTM) process. The other type of irregularities bear the characteristics of having been produced by medium-scale travelling ionospheric disturbance (MSTIDs) typically observed at mid-latitudes. In this latter case, the role of medium scale gravity waves in the irregularity generation appears to be evident. Gadanki radar observation of the F-region field aligned irregularities (FAI) in summer month by Patra *et al.*[61] showed dominant occurrence of the irregularities in post-midnight hours with characteristics often similar to those of the equinoctial decaying post-midnight FAI's. They proposed the gradient and R-T instabilities with Es providing important free energy as possible source of these irregularities. The different results, so far published, on the post-midnight spread F irregularities have been based on different types of observational techniques. From a morphological perspective, it appears that while a part (which appears rather small) of the cases of irregularity development may be attributed to R-T mechanism, the majority cases of the irregularity generation would appear to be driven by a mechanism similar to the one invoked to explain the pre-sunrise spread F over Fortaleza[60], because the F-region bottom-side undulations associated with the irregularities, in the latter case, do seem to have characteristics similar to those of the MSTIDs.

6 Discussions

The main objective of this paper is to present a brief overview and a discussion on nighttime F-region irregularities during solar minimum conditions, the importance of which is highlighted by the prolonged duration of the inactive sun that characterized the solar minimum phase of the cycle 23-24. It is noted that there are clear and basic differences in the characteristics of the irregularity occurrences in terms of their local time and seasonal/longitude distributions between the solar maximum and minimum years. During solar maximum, the irregularity development begins in the early post-sunset hours near 1900-2000 hrs LT, that is generally tied to the pre-reversal vertical drift that usually has large amplitudes, and the irregularities peak around 2200 hrs LT. The season/longitude distribution of the irregularities is influenced dominantly by longitudinal variation in magnetic declination angle[6,13]. In contrast, during solar minimum the irregularity development beginning near midnight and post-midnight hours dominate the occurrence pattern. Any influence in them from the magnetic declination angle can often be less clear. The seasonal/longitudinal distribution pattern of the midnight-post-midnight irregularities is also different from that of solar maximum epoch, in the sense that gravity wave influence appears to stand out in their distribution pattern (during solar minimum).

As pointed out above, the role of gravity wave influence in spread F initiation is clearly evident when the PRE amplitude is comparatively small. Figure 8(a) (Ref. 47) shows the evening vertical drift (PRE) velocity variation as a function of solar flux (F10.7), which is compared with the IRI model[62]. The vertical drift, here, was obtained from digisonde data over Sao Luis. Systematic decrease towards solar minimum in the vertical drift over Sao Luis may be noted in both observational and model results. The measured vertical drift is systematically higher than that predicted empirically for all solar flux values. However, it may be pointed out that the statistics of the observational data used in the analysis is rather poor for the low flux values, and therefore, the mean Vzp values of the solar minimum may be an over estimate. It is, therefore, reasonable to take the mean of the model and observational values as representing the vertical drift over Fortaleza during solar minimum. Thus, a vertical drift of ~ 20 m s^{-1} may be representative for a solar minimum with F10.7 of the

order of 70 flux unit that represented the recent prolonged solar minimum.

From the results in Fig. 8(b) (Ref. 63) that illustrate the control of the Vzp on the spread F intensity, it is clear that the latter is weak or the spread F is totally absent for small Vzp values of the order of 20 m s^{-1}, whereas the spread F intensity is high for large Vzp values. As discussed earlier and especially based on the results in Figs 5(a and b), it can be noted that the GW influence as precursor seed for spread F growth becomes clearly noticeable for low Vzp values of the order of 20 m s^{-1}, whereas for large Vzp values such

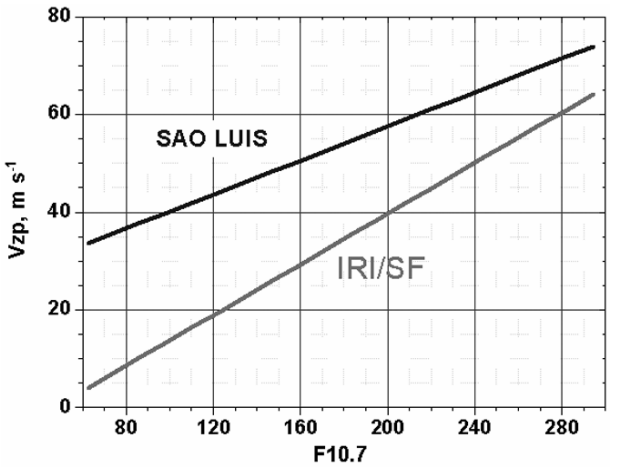

Fig. 8(a) — Pre-reversal vertical drift variation with solar flux (F10.7) over Sao Luis as obtained from digisonde, compared with the empirical model results of Scherliess & Fejer[62] implemented in the IRI scheme (Abdu *et al.*[47])

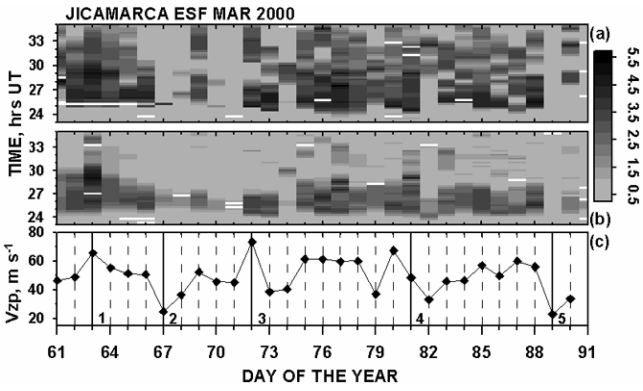

Fig. 8(b) — Equatorial spread F intensity from ionograms quantified (as a rough indicator) in terms of the range of the echo spreading (one unit representing 100 km of range spreading) is shown in the top and middle panels (white areas mark missing data) [top panel shows the echo spreading intensity at the higher frequency range of the F-layer trace and in the middle panel is plotted similar parameter for the lower frequency range; bottom panel shows the corresponding Vzp variations; dataset is for March 2000 over Jicamarca (Abdu *et al.*[63])

GW role is less conspicuous. This suggests the possibility of a trend for an anti-correlation between the PRE intensity and GW amplitude that determine the initiation and growth of the spread F instability process, which needs to be further confirmed from more analysis of observational data. The plausible causes of such a relationship can be visualized based on the following reasoning.

Tropospheric convective activity is a widely believed source of gravity waves (GWs) that propagate upward dissipating energy and momentum at F-region heights. This belief is based on theoretical/model calculations on the upward propagation characteristics of such GWs[36,50] as well as from statistical correlation found between global distribution of tropospheric active regions, represented by the ITCZ, and the global ESF occurrence pattern[22,33]. If the tendency for a reduced GW intensity with increasing F-layer height and PRE represents a real trend (which is under further investigation), it would offer the following possible scenario of conditions for the GW propagation into the F-layer bottom side:

1 The tropospheric GWs dissipating energy and momentum in the thermosphere begin loosing intensity with increasing height in the height region spanned by the post-sunset F-layer rise so that a higher (lower) F-layer height would correspond to a lower (higher) GW intensity; and /or

2 The GWs loose energy by interaction with the background zonal wind as shown from model calculations by Kherani *et al.*[35]. The background zonal wind (which is eastward in the evening) is known to drive the PRE so that a larger (smaller) zonal wind responsible for a stronger (weaker) PRE could result in higher (smaller) degree of weakening of the GW amplitude. It is important to conduct more studies towards clarifying these issues.

The low PRE vertical drift velocity that characterize the solar minimum conditions causes slowing down of the post-sunset instability build up, possibly initiated by a gravity wave seed perturbation, so that the consequent density perturbation (irregularities) that may often be part of a slowly rising bubble structure takes longer time to reach the F-layer topside. In this way, the spread F onset could suffer certain delay, which can be more conspicuous in the case of irregularities observed *in situ* by

satellites. This point appears to be verifiable in the results from C/NOFS presented in Fig. 9 (adopted from Heelis *et al.*[64]), which show the distribution of medium-scale irregularities (scale sizes between 10 and 400 km) in the total ion density as measured by the C/NOFS satellite in the equatorial region in the height range of 400-500 km. The occurrence of irregularity with amplitude greater than 15% and their average amplitude and the total ion density are shown as a function of magnetic local time and longitude for northern summer solstice, winter solstice and equinoxes. It may be noticed that the occurrence frequency of the medium scale irregularities has maximum through midnight and post-midnight hours, which is in contrast to previous studies that indicated the maximum occurrence rate between 2100 and 2400 hrs LT for higher level of solar activity. The onset times are also delayed significantly (with rare exceptions) compared to higher level of solar activity. The earliest irregularity occurrence is near 1930 hrs LT in Brazilian-Atlantic sector in December solstice (northern winter). Although, it is still delayed with respect to the onset times at higher level of solar activity, the earlier occurrence time, seasonally and longitudinally, appears to reflect the influence of the large westward magnetic declination (-21°) and the

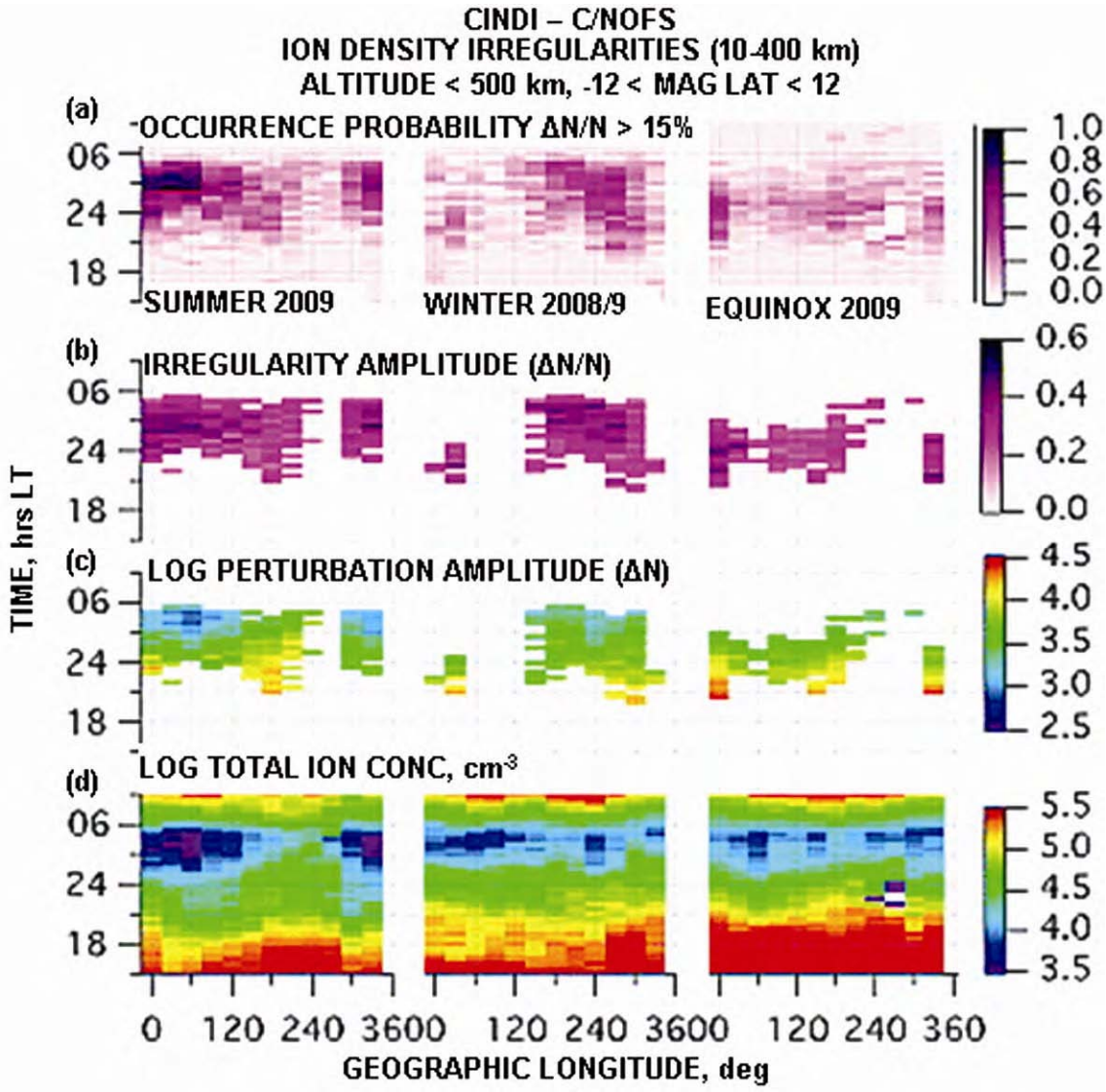

Fig. 9 — Average variations in local time and longitude of: (a) equatorial irregularity occurrence, (b) irregularity amplitude, (c) perturbation amplitude, and (d) total ion density [Results for northern summer, northern winter, and equinox are shown in columns from left to right (Heelis *et al.*[64])]

consequent sunset terminator - magnetic meridian alignment in this longitude sector in this part of the year[6,13]. Irrespective of such possible influences from magnetic declination, the generally, late onset of the irregularities, in all longitudes and seasons that is evident during the prolonged solar minimum of the observation period, is a clear indication of the dominating control in the irregularity development, by gravity wave seeding under the small post-sunset vertical drifts. Heelis *et al.*[64] suggested that the observed longitude and seasonal dependence in the peak occurrence frequency is influenced by seeding from tropospheric sources and therefore, responds to the seasonal variation in the co-location of the inter-tropical convergence zone (ITCZ) with respect to the dip equator.

Moving away in latitude from the dip equator, the irregularity growth and distribution are influenced by equatorial bubble processes as well as by thermospheric wave disturbances coming from mid latitudes. The role of medium scale travelling ionospheric disturbances (MSTID) in the distribution and dynamics of the midnight-post-midnight irregularities has been the subject of some recent investigations. The increase in occurrence, towards solar minimum, of post-midnight spread F over Cachoeira Paulista, a low latitude (equatorial anomaly) location in Brazil, discussed before, was explained as resulting from MSTID propagation from mid-latitudes[59]. However, a part of such occurrences may also be resulting from equatorial plasma bubbles development process. The features distinguishing the two types of the irregularity drivers were discussed recently by Yokoyama *et al.*[56,57] based on observational data from rapid beam steering by the Equatorial Atmosphere Radar (EAR) in Indonesia simultaneously with the CNOFS observations in the region. They showed sharp upwelling plumes near midnight which could not be a mere passage of fossil plasma bubble (meaning that they could be active bubbles) and the other was constituted of tilted structures presenting the same orientation as that of MSTID typically observed at mid-latitude. They proposed that the equator ward converging winds associated with the midnight temperature maximum (MTM) could play a role in the bubble instability growth near midnight. However, in this case as well, a possible role of equatorial GWs as seed perturbation cannot be ruled out. Thus, it appears that the GWs from either tropospheric convective sources (in the cases of post-sunset and near midnight equatorial bubbles/irregularities) or from mid-latitude MSTID (in the case of midnight to post-midnight irregularities at low altitudes) seem to govern the spread F irregularity distribution under solar minimum conditions.

7 Conclusions

This paper is intended to provide a brief overview on the current understanding of the equatorial spread F development focusing attention on the characteristics and variability of the irregularity occurrences, in terms of their local time, season and longitude distributions during solar activity minimum conditions. It has also been attempted to explain some well known features of the irregularity distribution based on the underlying mechanisms for the irregularity growth that are driven mainly by the two driving forces, the evening vertical drift /PRE and the GW seeding, and on the premise that the relative dominance of the driving forces varies considerably with the level of solar activity. The main points of the conclusions can be summarized as:

The evening F-layer vertical drift due to the pre-reversal enhancement in the zonal electric field (PRE) arising from sunset electrodynamics processes basically controls the post-sunset spread F /plasma bubble irregularity development. Observational evidence and model results clearly show that the PRE, depending upon its magnitude, can determine the intensity of the post-sunset spread F as well as the associated bubble rise velocity over the dip equator that sets the spread F onset time at off-equatorial latitudes. The role of precursor gravity waves in seeding the instability, through perturbations in density and polarization electric fields, appears well established for post-sunset events based on case studies and statistical analysis. From digisonde observations, it is seen that the role of a gravity wave seed to control the ESF instability growth is more easily observable when the PRE intensity is relatively small. While the evening vertical drift has larger amplitude at higher level of solar activity when it is the main determining factor in the post-sunset spread F growth, during solar minimum conditions the PRE is weaker and the role of precursor gravity waves in spread F development appears clearly observable. Further, during solar minimum, when the gravity wave forcing gains dominance relative to the PRE for instability growth, the spread F onset is generally delayed so that their midnight-post-midnight

occurrence characterizes the low level of solar activity. At low-latitude sites, post-midnight spread F have characteristics similar to those of the mid-latitude spread F believed to be produced by MSTIDs. It appears there are two broad classes of gravity waves that can be considered having deterministic roles in the spread F occurrences. One of them is invoked for events driven from dip equator wherein the seeding GWs could originate in tropospheric convective processes, and the other class is that identified as MSTIDs that appears to dominate the low latitude events. Further studies are needed to elucidate in greater detail the space-time distribution and the different generation mechanisms for the spread F irregularities in the equatorial-low-latitude regions under extremely low solar activity conditions.

Acknowledgements

The author wishes to acknowledge the support received from the Conselho Nacional de Desenvolvimento Cientifico e Tecnologico- CNPq through grants no 301214/2005-0 and 305028/2006-5. He also thanks Maria Goreti dos Santos Aquino for assistance in processing the digisonde/ionosonde data.

References

1 Booker H G & Wells H W, Scattering of radio waves in the F region of ionosphere, *Terr Magn Atmos Electr (USA)*, 43 (1938) 249.

2 Farley D T, Balsley B B & Woodman R F, Equatorial spread F – Implications VHF radar observations, *J Geophys Res (USA)*, 75 (1970) 7199.

3 Chandra H & Rastogi R G, Solar cycle and seasonal variation of spread-F near the magnetic equator, *J Atmos Terr Phys (UK)*, 32 (1970) 439, doi: 10.1016/0021-9169(70)90019-X.

4 Haerendel G, *Theory of equatorial spread F: Report* (Maxplanck-Institut fur Extraterres Phys Garching, Germany), 1973.

5 Woodman R F & LaHoz C, Radar observations of F region equatorial irregularities, *J Geophys Res (USA)*, 81 (1976) 5447.

6 Abdu M A, Bittencourt J A & Batista I S, Magnetic declination control of the equatorial F region dynamo field development and spread F, *J Geophys Res (USA)*, 86, (1981) 11443.

7 Abdu M A, Medeiros R T, Bittencourt J A & Batista I S, Vertical ionization drift velocities and range spread F in the evening equatorial ionosphere, *J Geophys Res (USA)*, 88 (1983) 399.

8 Abdu M A, Batista I S, Reinisch B W, de Souza J R, Sobral J H A, Bertoni F, Pedersen T R, Medeiros A F, Schuch N J & de Paula E R, Conjugate Point Equatorial Experiment (COPEX) Campaign in Brazil: Electrodynamics highlights on spread F development conditions and day-to-day variability, *J Geophys Res (USA)*, 114 (2009a), doi: 10.1029/2008JA013749.

9 Sobral J H A, Abdu M A, Zamlutti C J & Batista I S, Association between plasma bubble irregularities and airglow disturbances over Brazilian low latitudes, *Geophys Res Lett (USA)*, 1 (1980) 980.

10 Rastogi R G, Seasonal variation of equatorial spread F in the American and Indian zones, *J Geophys Res (USA),* 85 (1980) 22.

11 Zalesak S T, Ossakow S L & Chaturvedi P K, Nonlinear equatorial spread F: The effect of neutral winds and background Pealersen conductivity, *J Geophys Res (USA)*, 87 (1982) 151.

12 Subbarao K S V & Krishnamurthy B V, Seasonal variations of equatorial spread-F, *Ann Geophys (France)*, 12 (1994) 33.

13 Tsunoda R T, Control of the seasonal and longitudinal occurrence of equatorial scintillations by the longitudinal gradient in integrated E region Pedersen conductivity, *J Geophys Res (USA)*, 90 (1985), doi: 10.1029/JA090iA01p00447.

14 Tsunoda R T, On seeding equatorial spread F during solstices, *Geophys Res Lett (USA)*, 37 (2010) L05102, doi: 10.1029/2010GL042576.

15 Sekar R, Suhashini R & Raghavarao R, Effects of vertical winds and electric fields in the nonlinear evolution of equatorial spread F, *J Geophys Res (USA)*, 99 (1994) 2205.

16 Huang C -S & Kelley M C, Nonlinear evolution of equatorial spread-F, 4: Gravity waves, velocity shear and day-to-day variability, *J Geophys Res (USA)*, 101 (1996) 24,523.

17 Sultan P J, Linear theory and modeling of the Rayleigh-Taylor instability leading to the occurrence of equatorial spread F, *J Geophys Res (USA)*, 101 (1996) 26875.

18 Fejer B G, Scherliess L & de Paula E R, Effects of the vertical plasma drift velocity on the generation and evolution of equatorial spread F, *J Geophys Res (USA)*, 104 (1999) 19,854.

19 Sastri J H, Abdu M A, Batista I S & Sobral J H A, Onset conditions of equatorial (range) spread F at Fortaleza, Brazil during the June solstice, *J Geophys Res (USA)*, 102 (A11) (1997) 24013.

20 Kil H & Heelis R A, Global distribution of density irregularities in the equatorial ionosphere, *J Geophys Res (USA)*, 103 (1998) 407.

21 Hysell D L & Burcham J D, JULIA radar studies of equatorial spread F, *J Geophys Res (USA)*, 103 (1998) 29,155.

22 McClure J P, Sing S, Bamgboye D K, Johnson F S & Kil Hyusub, Occurrence of equatorial F region irregularities: Evidence for tropospheric seeding, *J Geophys Res (USA)*, 103 (1998) 29119.

23 Prakash S, Production of electric filed perturbations by gravity wave winds in the E region suitable for initiating equatorial spread F*, J Geophys Res (USA)*, 104 (A5) (1999) 10051.

24 Abdu M A, Outstanding problems in the equatorial ionosphere-thermosphere system relevant to spread F, *J Atmos Sol-Terr Phys (UK)*, 63 (2001) 869.

25 Bhattacharyya A, Role of E region conductivity in the development of equatorial ionospheric plasma bubbles, *Geophys Res Lett (USA)*, 31 (2004), doi: 10.1029/2003GL018960.

26 Fukao S, Yokoyama T & Tayama T, Eastward traverse of equatorial plasma plumes observed with the Equatorial Atmosphere Radar in Indonesia, *Ann Geophys (Germany)*, 24 (5) (2006) 1411.

27 Thampi S V, Yamamoto M, Tsunoda R T, Otsuka Y, Tsugawa T, Uemoto J & Ishii M, First observations of large□scale wave structure and equatorial spread F using CERTO radio beacon on the C/NOFS satellite, *Geophys Res Lett (USA)*, 36, (2009) L18111, doi: 10.1029/ 2009GL039887.

28 Abdu M A, Sobral J H A, Nelson O R & Batista I S, Solar cycle related range type spread F occurrence characteristics over equatorial and low latitude stations in Brazil, *J Atmos Terr Phys (UK)*, 47 (1985) 901.

29 Fejer B G, de Paula E R, Gonzalez S A & Woodman R F, Average vertical and zonal F-region plasma drifts over Jicamarca, *J Geophys Res (USA)*, 96 (1991) 13901.

30 Maruyama T & Matuura N, Longitudinal variability of annual changes in activity of equatorial Spread F and plasma bubbles, *J Geophys Res (USA)*, 89 (A12) (1984) 10,903.

31 Abdu M A, Batista I S & Sobral J H A, A new aspect of magnetic declination control of equatorial spread F and F region dynamo, *J Geophys Res (USA)*, 97 (1992) 14897.

32 Batista I S, Abdu M A & Bittencourt J A, Equatorial F-region vertical plasma drifts: Seasonal and longitudinal asymmetries in the American sector, *J Geophys Res (USA)*, 91 (1986) 12,055.

33 Rottger J, Equatorial spread F by electric fields and atmospheric gravity waves generated by thunderstorms, *J Atmos Terr Phys (UK)*, 43 (1981) 453.

34 Abdu M A, Kherani E A, Batista I S, de Paula E R, Fritts D C & Sobral J H A, Gravity wave initiation of equatorial spread F/plasma bubble irregularities based on observational data from the SpreadFEx campaign, *Ann Geophys (Germany)*, 27 (2009b) 1.

35 Kherani E A, Abdu M A, de Paula E R, Fritts D C, Sobral J H A & de Meneses Jr F C, The impact of gravity waves rising from convection in the lower atmosphere on the generation and nonlinear evolution of equatorial bubble, *Ann Geophys (Germany)*, 27 (2009) 1657.

36 Fritts D C, Vadas S L, Riggin D M, Abdu M A, Batista I S, Takahashi H, Medeiros A, Kamalabadi F, Liu H -L, Fejer B G & Taylor M J, Gravity wave and tidal influences on equatorial spread F based on observations during the Spread F Experiment (SpreadFEx), *Ann Geophys (Germany)*, 26 (2008) 3235.

37 Rishbetheth H, Polarization fields produced by winds in the equatorial F region, *Planet Space Sci (UK)*, 19 (1971) 357.

38 Heelis R A, Kendall P C, Moffet R J, Windle D W & Rishbeth H, Electrical coupling of the E- and F- region and its effects on the F-region drifts and winds, *Planet Space Sci (UK)*, *22* (1974) 743.

39 Farley D T, Bonelli E, Fejer B G & Larsen M F, The pre-reversal enhancement of the zonal electric field in the equatorial ionosphere, *J Geophys Res (USA)*, 91 (1986) 13,723.

40 Yokoyama T, Fukao S & Yamamoto M, Relationship of the onset of equatorial F region irregularities with the sunset terminator observed with the Equatorial Atmosphere Radar, *Geophys Res Lett (USA),* 31 (2004) L24804, doi: 10.1029/2004GL021529.

41 Maruyama T, A diagnostic model for equatorial spread F, 1: Model description and application to electric field and neutral wind effects, *J Geophys Res (USA)*, 93 (1988) 14611.

42 Keskinen M J, Ossakow S L & Fejer B G, Three-dimensional nonlinear evolution of equatorial spread-F bubbles, *Geophys Res Lett (USA)*, 30 (16) (2003) 1855, doi: 10.1029/ 2003GL017418.

43 Abdu M A, Batista P P, Batista I S, Brum C G M, Carrasco A J & Reinisch B W, Planetary wave oscillations in mesospheric winds, equatorial evening pre-reversal electric field and spread F, *Geophys Res Lett (USA)*, 33 (2006a), doi: 10.1029/2005GL024837.

44 Su S Y, Chao C K & Liu C H, On monthly/ seasonal/longitudinal variations of equatorial irregularity occurrences and their relationship with the post-sunset vertical drift velocities, *J Geophys Res (USA)*, *113* (2008) A05307, doi: 10.1029/2007JA012809.

45 Chapagain N P, Fejer B G & Chau J L, Climatology of post sunset equatorial spread F over Jicamarca, *J Geophys Res (USA)*, 114 (2009), doi: 10.1029/2008JA013911.

46 Namboothiri S P, Balan N & Rao P B, Vertical plasma drifts in the F region at the magnetic equator, *J Geophy Res (USA)*, 94 (A9) (1989) 12,055.

47 Abdu M A, Batista I S, Brum C G M, MacDougall J W, Santos A M, de Souza J R & Sobral J H A, Solar flux effects on the equatorial evening vertical drift and meridional winds over Brazil: A comparison between observational data and the IRI model and the HWM representations, *Adv Space Res (UK)*, 46 (2010) 1078.

48 Anderson D N, Reinisch B W, Valladares C, Chau J & Veliz O, Forecasting the occurrence of ionospheric scintillation activity in the equatorial ionosphere on a day-to-day basis, *J Atmos Sol-Terr Phys (UK)*, 66 (2004) 1567, doi: 10.1016/j.jastp.2004.07.010.

49 Fritts D C & Vadas S L, Gravity wave penetration into the thermosphere: Sensitivity to solar cycle variations and mean winds, *Ann Geophys (Germany*), 26 (2008) 3841.

50 Vadas S L & Liu H –L, The generation of large-scale gravity waves and neutral winds in the thermosphere from the dissipation of convectively-generated gravity waves, *J Geophys Res (USA)*, 114 (2009) A10310, doi: 10.1029/2009JA014108.

51 Kelley M C, Larsen M F & LaHoz C, Gravity wave initiation of equatorial spread-F: A case study, *J Geophys Res (USA)*, 86 (1981) pp 9087–9100.

52 Kudeki E, Akgiray A, Milla M, Chau J L & Hysell D L, Equatorial spread-F initiation: post-sunset vortex, thermo spheric winds, gravity waves, *J Atmos Sol-Terr Phys (UK)*, 69 (2007) 2416.

53 Abdu M A, Iyer Krishna Narayana, Medeiros R T de, Batista Inez S & Sobral Jose H A, Thermospheric meridional wind control of equatorial spread F and evening pre-reversal electric field, *Geophys Res Lett (USA)*, 33 (2006b) 1.

54 Sastri J H, Post-midnight onset of spread-F at Kodaikanal during the June solstice of solar minimum, *Ann Geophys (France)*, 17 (1999) 1111.

55 Niranjan K, Brahmanandam P S, Ramkrishnarao P, Uma G, Prasad D S V V D & Ramarao P V S, Post midnight spread-F occurrence over Waltair (17.7^{o}N, 83.3^{o}E) during low and ascending phases of solar activity, *Ann Geophys (Germany)*, 21 (2003) 745.

56 Yokoyama T, Yamamoto M, Otsuka Y, Nishioka M, Tsugawa T, Watanabe S & Pfaff R F, On post midnight low‐latitude ionospheric irregularities during solar minimum, 1: Equatorial Atmosphere Radar and GPS‐TEC observations in Indonesia, *J Geophys Res (USA)*, 116 (2011a) A11325, doi: 10.1029/2011JA016797.

57 Yokoyama T, Pfaff R F, Roddy P A, Yamamoto M & Otsuka Y, On post midnight low□latitude ionospheric irregularities during solar minimum, 2: C/NOFS observations and comparisons with the Equatorial Atmosphere Radar, *J Geophys Res (USA)*, 116 (2011b) A11326, doi: 10.1029/2011JA016798.

58 Li G, Ning B, Abdu M A, Yue X, Liu L, Wan W & Hu L, On the occurrence of post-midnight equatorial F region irregularities during the June solstice, *J Geophys Res (USA)*, 116 (2011) A04318, doi: 10.1029/2010JA016056.

59 Candido C M N, Batista I S, Becker-Guedes F, Abdu M A, Sobral J H A & Takahashi H, Spread F occurrence over a southern anomaly crest location in Brazil during June solstice of solar minimum activity, *J Geophys Res (USA)*, 116 (2011), doi: 10.1029/2010JA016374.

60 MacDougall J W, Abdu M A, Jayachandran P T, Cecile J -F & Batista I S, Pre sunrise spread F at Fortaleza, *J Geophys Res (USA)*, 103 (A10) (1998) 23415.

61 Patra A K, Phanikumar D V & Pant T K, Gadanki radar observations of F region field-aligned irregularities during June solstice of solar minimum: First results and preliminary analysis, *J Geophys Res (USA)*, 114 (2009) A12305, doi: 10.1029/2009JA014437.

62 Scherliess L & Fejer B G, Radar and satellite global equatorial F region vertical drift model, *J Geophys Res (USA)*, 104 (A4) (1999) 6829.

63 Abdu M A, Ramkumar T K, Batista I S, Brum C G M, Takahashi H, Reinisch B W & Sobral J H A, Planetary wave signatures in the equatorial atmosphere–ionosphere system, and mesosphere- E- and F-region coupling, *J Atmos Sol-Terr Phys (UK)*, 68 (2006c) 509.

64 Heelis R A, Stoneback R, Earle G D, Haaser R A & Abdu M A, Medium‐scale equatorial plasma irregularities observed by Coupled Ion‐Neutral Dynamics Investigation sensors aboard the Communication Navigation Outage Forecast System in a prolonged solar minimum, *J Geophys Res (USA)*, 115 (2010) A10321, doi: 10.1029/2010JA015596.